

Non-Bloch self-energy of dissipative interacting fermions

He-Ran Wang,^{1,*} Zijian Wang,^{1,*} and Zhong Wang^{1,†}

¹*Institute for Advanced Study, Tsinghua University, Beijing 100084, People's Republic of China*

The non-Hermitian skin effect describes the phenomenon of exponential localization of single-particle eigenstates near the boundary of the system. We explore its generalization to the many-body regime by investigating interacting fermions in open quantum systems. Therein, the elementary excitations from the “vacuum” (steady state) are given by two types of dissipative quasi-particles composed of single-fermion operators. We perturbatively calculate the self-energy of these quasi-particles in the presence of interactions, and utilize the non-Bloch band theory to develop an exact integral formula, which is further simplified by imposing complex momentum conservation. The formula allows calculating the Liouvillian gap modified by interactions with high precision, as demonstrated by comparison to numerical results. Furthermore, our results show that interactions can even enhance the non-reciprocity of fermion hoppings, contrary to the conventional viewpoint from the Pauli exclusion principle. Our formulation provides a quantitative tool for investigating dissipative interacting fermions with non-Hermitian skin effect, and generalizes the Fermi liquid theory to open quantum systems in the context of diagrammatic perturbation theory.

Introduction—When a quantum system interacts with the environment, an accurate description of its dynamics requires incorporating non-Hermiticity into the unitary evolution. In recent years, numerous intriguing phenomena have been discovered in open quantum systems and non-Hermitian models. Among these, the non-Hermitian skin effect (NHSE) in one-dimensional (1D) models has attracted considerable attention [1–11]. The hallmark of NHSE is the unusual behavior of eigenstates, that they accumulate exponentially near the boundary under the open boundary condition (OBC), in contrast to the homogeneous distribution along the chain under periodic boundary condition (PBC). Despite the explicit breaking of translational invariance, the eigenstates can be labeled by complex momentum with nonzero imaginary part, according to the recently established non-Bloch band theory [1, 12–22]. All the complex momenta of eigenstates form closed curves on the complex plane, which is dubbed the generalized Brillouin zone (GBZ) [1, 12, 17, 23].

The extensions of single-particle NHSE to the many-body regime could give rise to novel phases of matter [24–34]. The characterization of many-body topological phases in the presence of NHSE requires proper generalizations of closed-system topological indicators [35–42]. On the other hand, many-body interactions can become the source of NHSE (e.g. through non-Hermitian self-energy [43–48], integrable interparticle scattering [49–51], or density-assisted non-reciprocal hoppings [52–55]). Various analytical and numerical techniques have been introduced to address the many-body problem in this context, including non-Hermitian Bethe ansatz [49–51, 56, 57] and tensor network techniques [34, 40, 58, 59]. However, a systematic understanding of the interplay between interactions and generic NHSE models is still lacking hitherto, particularly regarding the role of GBZ in many-body physics.

In this paper, we make progress on this subject within the framework of Lindblad master equation, which describes the Markovian open quantum system dynamics [60],

$$\frac{d\rho}{dt} = -i[H, \rho] + \sum_{\mu} (2L_{\mu}\rho L_{\mu}^{\dagger} - \{L_{\mu}^{\dagger}L_{\mu}, \rho\}) \equiv \mathcal{L}\rho,$$

where ρ denotes the density matrix, H is the Hamiltonian, L_{μ} are the jump operators with index μ running over all channels coupled to the environment, and \mathcal{L} is the Liouvillian superoperator. Here, we consider a class of 1D fermionic Liouvillians, which possess a non-interacting part \mathcal{L}_0 exhibiting Liouvillian skin effect [61–64], along with four-fermion interactions \mathcal{L}_I . In this theoretical set up, the non-Hermiticity arises from the full-fledged Liouvillian, where many-body interactions are included naturally. The non-interacting part is diagonalized through the fermionic bi-base mapping method [65], resulting in two types of dissipative quasi-particles. The interactions are then transformed to quasi-particle pairing terms, and we perturbatively project them into the single-particle subspace as the self-energy. The original form of the perturbative self-energy involves triple integrals over the GBZ, thus posing challenges to direct numerical calculations. We develop a Feynman diagram method to resolve the problem. By introducing the notion of complex momentum conservation, we simplify the formula of non-Bloch self-energy to double integrals over the conventional Brillouin zone (BZ). We demonstrate our method by investigating a Liouvillian version of the Hatano-Nelson model. From the matrix elements of single-particle self-energy, it is shown that the non-reciprocity is enhanced by weak interaction. Furthermore, we show the accuracy and validity of our approach through the comparison with numerical results on the Liouvillian gap in the presence of interactions. Our formulation can be viewed as an open-system generalization of the Fermi liquid theory in the framework of diagrammatic perturbation, in the sense that interaction dresses the free particles into quasi-particles.

Fermionic double-base mapping—The non-interacting Liouvillian consists of a quadratic Hamiltonian $H = \sum_{ij} h_{ij} c_i^{\dagger} c_j$, and single particle dissipators $L_{\mu}^l = \sum_i D_{\mu i}^l c_i$, $L_{\mu}^g = \sum_i D_{\mu i}^g c_i^{\dagger}$, where $c_i^{\dagger} (c_i)$, $i = 1, \dots, N$ are fermionic creation (annihilation) operators defined on a 1D lattice. By applying the double-base mapping, we map the density matrix to a vector [65]: $\rho = \sum_{m,n} \rho_{mn} |m\rangle \langle n| \rightarrow \rho = \sum_{m,n} \rho_{mn} |m\rangle \otimes |n\rangle$,

with basis states $|m\rangle = |m_1, \dots, m_N\rangle$, $|n\rangle = |\bar{n}_1, \dots, \bar{n}_N\rangle$. $m_i(\bar{n}_i)$ represents fermion number on the site i . Consequently, the non-interacting Liouvillian \mathcal{L}_0 admits the bilinear form:

$$\begin{aligned} \mathcal{L}_0 &= \mathbf{c}^\dagger \mathbb{L}_0 \mathbf{c} - \text{Tr}[M^l + (M^g)^T - ih], \\ \mathbb{L}_0 &= \begin{pmatrix} -ih + (M^g)^T - M^l & 2(M^g)^T \\ 2M^l & -ih - (M^g)^T + M^l \end{pmatrix}. \end{aligned} \quad (1)$$

Here, we introduce the matrices: $M_{ij}^{g(l)} = \sum_\mu D_{\mu i}^{g(l)*} D_{\mu j}^{g(l)}$, and the Nambu basis of left and right fermions: $\mathbf{c} = (\eta c_1, \dots, \eta c_N, \bar{c}_1^\dagger \bar{\eta}, \dots, \bar{c}_N^\dagger \bar{\eta})^T$, where the fermion parity operator $\eta = \exp(i\pi \sum_i n_i)$ is used to restore the anti-commutation relations between fermionic operators originally acting on different sides of ρ [66]. We then introduce a similarity transformation S to block diagonalize \mathbb{L}_0 as $S \mathbb{L}_0 S^{-1} = \begin{pmatrix} -X^\dagger & \\ & X \end{pmatrix}$. The diagonal block $X = -ih - (M^g)^T - M^l$ is the damping matrix [61], which encodes complete information of the Liouvillian spectrum. The similarity transformation matrix admits the form $S = \frac{1}{\sqrt{2}} \begin{pmatrix} I & I \\ I + Z & -I + Z \end{pmatrix}$, with Z being determined by the block-diagonal condition $XZ + ZX^\dagger = 2(M^g)^T - 2M^l$ (see Supplementary Materials [67] for more details). Then, we can define two types of decoupled quasi-particle operators:

$$(\mathbf{b}_R^\dagger, \mathbf{a}_L)^T = S \mathbf{c}, \quad (\mathbf{b}_L, \mathbf{a}_R^\dagger) = \mathbf{c}^\dagger S^{-1}. \quad (2)$$

The subscript $R(L)$ denotes right (left), and the corresponding quasi-particle operators satisfy mutual anti-commutation relations: $\{a_{Ri}^\dagger, a_{Lj}\} = \{b_{Ri}^\dagger, b_{Lj}\} = \delta_{ij}$, $\{a_{Ri}, b_{Rj}\} = \{a_{Li}, b_{Lj}\} = 0$. Then the non-interacting Liouvillian is represented as $\mathcal{L}_0 = \mathbf{a}_R^\dagger X \mathbf{a}_L + \mathbf{b}_R^\dagger X^* \mathbf{b}_L$, where the quasi-particle vacuum corresponds to the non-equilibrium steady state of Liouvillian. We are particularly interested in the eigenvalue of X with the largest real part, which corresponds to the lowest decay rate of quasi-particle excitations, representing the Liouvillian gap [see Fig. 1(a) for a pictorial illustration].

Self-energy and Feynman diagram— To incorporate density-density interactions $H_I = \sum_{\langle ij \rangle} U_{ij} n_i n_j$ into the non-interacting Liouvillian, we represent the interacting Liouvillian $\mathcal{L}_I = -i \sum_{\langle ij \rangle} U_{ij} (n_i n_j - \bar{n}_i \bar{n}_j)$ by quasi-particle operators. For simplicity, balanced gain and loss is assumed: $(M^g)^T = M^l$, hence $Z = 0$ and $a_{Ri} = a_{Li} = a_i, b_{Ri} = b_{Li} = b_i$. The interacting Liouvillian can be written as

$$\begin{aligned} \mathcal{L}_I &= -i \sum_{\langle ij \rangle} U_{ij} \left[\frac{1}{4} (a_i^\dagger a_i + a_j^\dagger a_j - b_i^\dagger b_i - b_j^\dagger b_j) \right. \\ &\quad \left. + \frac{1}{2} (a_i^\dagger b_i^\dagger + b_i a_i) (a_j^\dagger a_j - b_j^\dagger b_j) + \text{H.c.} \right]. \end{aligned} \quad (3)$$

Our method is also applicable to models with generic Z [67].

Notice that terms contributed by the interacting Liouvillian can be classified into two kinds: terms diagonal in quasi-particle Fock-state basis, and quasi-particle pairing interactions. The diagonal terms are purely imaginary and have

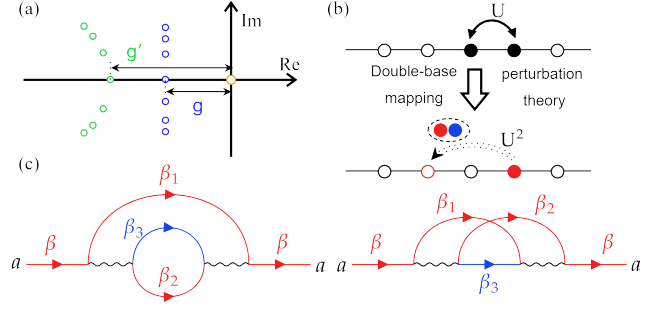


FIG. 1. (a) A sketch of Liouvillian spectrum. Blue (green) circles correspond to the model with (without) interactions, and g (g') is the gap. Only eigenvalues close to the imaginary axis are presented. The orange circle located at zero corresponds to the steady state. (b) A schematic plot about the self-energy. Interactions between fermions (black dots) with strength U are mapped to the doublon-assisted hopping of a quasi-particle (red dot). (c) Feynman diagrams of the second-order self-energy. Red (blue) lines correspond to the a (b)-particle, labeled by its complex momentum; wavy lines denote interactions.

no influence on the Liouvillian gap. Therefore, we focus on the pairing interactions, which do not conserve quasi-particle numbers. In the case of weak interactions, we can adopt the standard perturbation theory to the second order to effectively approximate the pairing potential by the self-energy:

$$\mathcal{L}_{\text{eff}}(E) = P \mathcal{L}_0 P + P \mathcal{L}_I P + P \mathcal{L}_I Q (E - Q \mathcal{L}_0 Q)^{-1} Q \mathcal{L}_I P + \dots \quad (4)$$

Here $P = I - Q$ is the projector of the Hilbert subspace of one a -particle, since the lowest decaying modes typically reside in this subspace. Therefore, the self-energy is generated through the following procedure [see Fig. 1(b) for a pictorial illustration]: (1) Creating a pair of quasi-particles (doublon) on the same site, (2) propagating three particles, (3) annihilating a doublon on another site.

To obtain a closed-form representation of the self-energy matrix elements, we label the basis of single-particle states as $|i_a\rangle = a_i^\dagger |0\rangle$, and that of intermediate three-particle states as $|i_a, j_a, k_b\rangle$. The zeroth order Liouvillian is simply given by the damping matrix $\langle i_a | \mathcal{L}_0 | j_a \rangle = X_{ij}$. The first order correction comes from the diagonal term in Eq. (3): $\langle i_a | \mathcal{L}_I | j_a \rangle = -\frac{i}{4} \delta_{ij} \sum_k U_{ik}$. From now on, we assume translational invariance for the damping matrix and interactions: $X_{ij} = X_{i-j}, U_{ij} = U_{i-j}$. The evaluation of the second order terms is one of the main theoretical results of our work:

$$\begin{aligned} &\langle i_a | \mathcal{L}_{\text{eff}}^{(2)}(E) | j_a \rangle \\ &= -\frac{1}{4} \sum_{kl} U_{ik} U_{jl} \langle i_a, k_a, k_b | (E - Q \mathcal{L}_0 Q)^{-1} | j_a, l_a, l_b \rangle \\ &= -\frac{1}{4} \sum_{kl} U_{ik} U_{jl} \oint_{\text{GBZ}} \frac{d\beta_1}{2\pi i \beta_1} \oint_{\text{GBZ}} \frac{d\beta_2}{2\pi i \beta_2} \oint_{\text{GBZ}^*} \frac{d\beta_3}{2\pi i \beta_3} \\ &\quad \frac{(\beta_1^{i-j} \beta_2^{k-l} - \beta_1^{i-l} \beta_2^{k-j}) \beta_3^{k-l}}{E - X(\beta_1) - X(\beta_2) - X^*(\beta_3)}. \end{aligned} \quad (5)$$

From the second to the third line, we apply the GBZ-based formula of the Green's function [20] to evaluate the propagator in the three-particle subspace. Note that $X^*(\beta)$ denotes the complex conjugate of all coefficients of the polynomial $X(\beta)$, but not of the variable β , and GBZ* is the complex conjugate of GBZ. The two terms in the numerator originate from the indistinguishability of two a -particles, while the fermionic statistics accounts for the minus sign in between. Notice that although translational symmetry is broken by the presence of boundaries, the self energy matrix elements deep in the bulk still respect that symmetry. Therefore, we can define the *non-Bloch self-energy* $\Sigma^{(2)}(E, \beta)$ as a Laurent polynomial of β ,

$$\begin{aligned} \Sigma^{(2)}(E, \beta) &\equiv \sum_r \beta^{-r} \langle (i+r)_a | \mathcal{L}_{\text{eff}}^{(2)} | i_a \rangle \\ &= -\frac{1}{4} \oint_{\text{GBZ}} \frac{d\beta_1}{2\pi i \beta_1} \oint_{\text{GBZ}} \frac{d\beta_2}{2\pi i \beta_2} \oint_{\text{GBZ}^*} \frac{d\beta_3}{2\pi i \beta_3} \sum_r \left(\frac{\beta_1 \beta_2 \beta_3}{\beta} \right)^r \\ &\quad \times \frac{U(\beta_2 \beta_3)^2 - U(\beta_2 \beta_3)U(\beta_1 \beta_3)}{E - X(\beta_1) - X(\beta_2) - X^*(\beta_3)}, \end{aligned} \quad (6)$$

where $U(\beta) = \sum_r \beta^{-r} U_r$. Furthermore, we uncover the Feynman diagrammatic representation [Fig. 1(c)] of the formula by rewriting the denominator as a virtual time integral

$$\begin{aligned} \Sigma^{(2)}(E, \beta) &= -\frac{1}{4} \sum_r \oint_{\text{GBZ}} \frac{d\beta_1}{2\pi i \beta_1} \oint_{\text{GBZ}} \frac{d\beta_2}{2\pi i \beta_2} \oint_{\text{GBZ}^*} \frac{d\beta_3}{2\pi i \beta_3} \\ &\quad \left(\frac{\beta_1 \beta_2 \beta_3}{\beta} \right)^r [U(\beta_2 \beta_3)^2 - U(\beta_2 \beta_3)U(\beta_1 \beta_3)] \\ &\quad \times \int_0^\infty dt \exp[-(E - X(\beta_1) - X(\beta_2) - X^*(\beta_3))t] \\ &= -\frac{1}{4} \oint_{\text{GBZ}} \left(\frac{d\beta_1}{2\pi i \beta_1} \frac{d\beta_2}{2\pi i \beta_2} \frac{d\beta_3}{2\pi i \beta_3} \right) \sum_r \left(\frac{\beta_1 \beta_2 \beta_3}{\beta} \right)^r \\ &\quad \times \int_0^\infty dt \int_0^{2\pi} \left(\frac{d\omega_1}{2\pi} \frac{d\omega_2}{2\pi} \frac{d\omega_3}{2\pi} \right) \exp[(i\omega_1 + i\omega_2 + i\omega_3 - E)t] \\ &\quad \times V(\beta_1, \beta_2, \beta_3) G_a(i\omega_1, \beta_1) G_a(i\omega_2, \beta_2) G_b(i\omega_3, \beta_3). \end{aligned} \quad (7)$$

Here, the single-particle propagators are $G_a(i\omega, \beta) = (i\omega - X(\beta))^{-1}$, $G_b(i\omega, \beta) = (i\omega - X^*(\beta))^{-1}$, and the interaction vertex is $V(\beta_1, \beta_2, \beta_3) = U(\beta_2 \beta_3)^2 - U(\beta_2 \beta_3)U(\beta_1 \beta_3)$. In the Feynman diagram [Fig. 1(c)], there are *external vertices* where a single particle line splits into one particle line and one interaction line. On the other hand, at *internal vertices*, one interaction line transfers momentum to two particle lines, where the conservation law of complex momentum manifests automatically.

Our self-energy formula (6) can be applied to calculate the non-Bloch self-energy as a Laurent polynomial of β to any desired power given the shape of GBZ. However, a generic GBZ is analytically non-tractable, obstructing accurate calculations of integrals on the GBZ. We overcome the difficulty by changing the integral contours from GBZ to BZ and imposing complex momentum conservation on the *external*

vertices. Concretely, first we deform the integral contours of β_1 and β_2 to the BZ, and the contour of β_3 to the circle with a specific radius $|\beta_3| = |\beta/(\beta_1 \beta_2)|$. In the time-integral form of self-energy [the first equality of Eq. (7)], these deformations are justified because the only singularity of the integrand lies at the original point [44]. Then the summation over r in the self-energy formula is reduced to $\sum_r (\beta_1 \beta_2 \beta_3 / \beta)^r = 2\pi i \beta_3 \delta(\beta_3 - \beta / \beta_1 \beta_2)$, implying the complex momentum conservation at the external vertices. Consequently, instead of triple integrals on the GBZ, we only need to calculate the following double integrals on the BZ:

$$\begin{aligned} \Sigma^{(2)}(E, \beta) &= -\frac{1}{4} \oint_{\text{BZ} \otimes 2} \frac{d\beta_1}{2\pi i \beta_1} \frac{d\beta_2}{2\pi i \beta_2} V(\beta_1, \beta_2, \beta / \beta_1 \beta_2) \\ &\quad \times \int_0^\infty dt \exp[-(E - X(\beta_1) - X(\beta_2) - X^*(\beta / \beta_1 \beta_2))t] \\ &= -\frac{1}{4} \int_0^{2\pi} \frac{dk_1}{2\pi} \int_0^{2\pi} \frac{dk_2}{2\pi} V(e^{ik_1}, e^{ik_2}, \beta e^{-ik_1 - ik_2}) \\ &\quad \times [(E - X(e^{ik_1}) - X(e^{ik_2}) - X^*(\beta e^{-ik_1 - ik_2}))^{-1}]. \end{aligned} \quad (8)$$

We emphasize that only when the denominator in Eq. (6) and Eq. (8) both have a positive real part, one can rewrite it as a virtual time integral. Conceptually, the conditions of positivity can be demonstrated as the stability of quasi-particle under perturbation, where the creation of a doublon costs finite ‘‘energy’’, thus contributing to the self-energy as virtual creation and annihilation processes.

To map out the perturbed non-Bloch band $E(\beta)$, one should solve the self-consistent integral equation $E(\beta) = E^{(0)}(\beta) + \Sigma^{(2)}(E(\beta), \beta)$, where $E^{(0)}(\beta) = X(\beta)$ is the non-Bloch band before adding perturbations. However, for weak interaction strength U , it suffices to have $E(\beta) = E^{(0)}(\beta) + \Sigma^{(2)}(E^{(0)}(\beta), \beta)$. Under OBC, each eigenstate is composed of $2M$ non-Bloch wave modes (M is the hopping range) with different β but the same energy $E_0(\beta)$: $|R\rangle = \sum_{\mu=1}^{2M} \sum_{i=1}^N \phi_\mu^R \beta_\mu^i |i\rangle$, $\langle L| = \sum_{\mu=1}^{2M} \sum_{i=1}^N \phi_\mu^L \beta_\mu^{-i} \langle i|$, where β_μ 's are sorted in increasing magnitude [1, 12]. To obtain self-energy corrections to an eigenstate, we need to decide which β to be taken. It turns out that one should calculate a weighted average of $\Sigma^{(2)}(E^{(0)}, \beta_M)$ and $\Sigma^{(2)}(E^{(0)}, \beta_{M+1})$ (see Supplementary Materials [67]):

$$\frac{\phi_M^R \phi_M^L \Sigma^{(2)}(E^{(0)}, \beta_M) + \phi_{M+1}^R \phi_{M+1}^L \Sigma^{(2)}(E^{(0)}, \beta_{M+1})}{\phi_M^R \phi_M^L + \phi_{M+1}^R \phi_{M+1}^L}. \quad (9)$$

Contributions from other complex momenta are of order $\mathcal{O}(1/N)$ at most.

Examples—To benchmark the efficiency and accuracy of our method, we apply the formula to a Liouvillian version [61] of Hatano-Nelson model [68–70] with nearest-neighbor interactions, in the context of open quantum systems. The corresponding Liouvillian consists of a quadratic Hamiltonian in the first-quantized form $h_{ij} = t(\delta_{i,j+1} + \delta_{i,j-1})$ and linear dissipators $L_j^l = \sqrt{\gamma/2}(c_j - ic_{j+1})$, $L_j^g = (L_j^l)^\dagger$. The non-Bloch damping matrix is $X(\beta) = -2\gamma - i(t -$

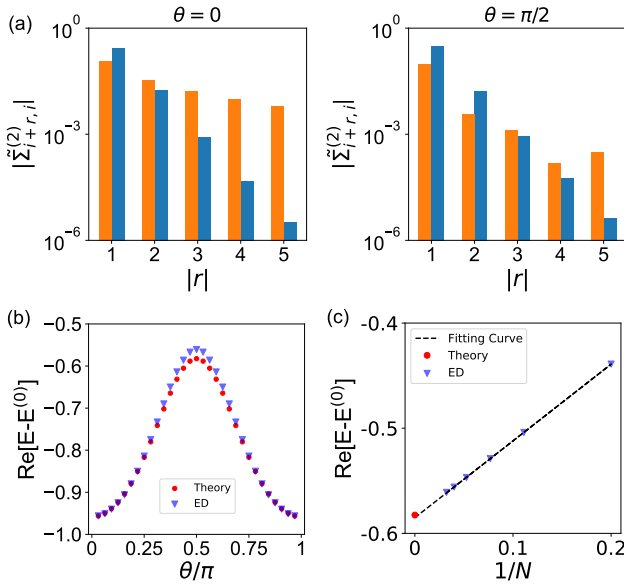


FIG. 2. Self-energy calculated through different methods. Parameters are $t = 1, \gamma = 0.5$, and energies are plotted in the unit of $u^2, u = 0.02$. (a) Interaction-induced hopping strength for different ranges r , which can be positive or negative, computed from triple integrals over the GBZ, scaled by $|\beta|^r$. Orange (blue) bars for positive (negative) r . $\theta = 0(\pi/2)$ on the left (right) panel refers to the angle of the input β . (b) The self-energy of eigenstates as the function of angle of β on GBZ. $E(E^{(0)})$ refers to eigenenergies after (before) adding perturbations. The largest real part appears at $\theta = \pi/2$, which determines the Liouvillian gap. The red dots come from integrals on the Brillouin zone, and the blue triangles denote results obtained from exact diagonalization (ED) of the Liouvillian by cutting off the whole Hilbert space to the subspace with one or three quasi-particles, $N = 31$. (c) Finite-size scaling of ED self-energy at $\theta = \pi/2$, which is extrapolated to the thermodynamic limit and approaches the analytical result (red point).

$\gamma)\beta - i(t + \gamma)\beta^{-1}$, and the interaction term is $U(\beta) = u(\beta + \beta^{-1})$. For $t > \gamma > 0$, the GBZ is a circle with a radius $\sqrt{(t + \gamma)/(t - \gamma)}$, allowing us to efficiently calculate integrals on both GBZ and BZ. The continuous spectrum of a -particle is $E^{(0)}(\theta) = -\gamma - 2i\sqrt{t^2 - \gamma^2}\cos(\theta), \theta \in [0, 2\pi)$, which shares the same real part. Therefore, after adding perturbations, the Liouvillian gap is determined by the eigenstate with the largest self-energy real part. Before proceeding, we emphasize that even for such a simple NHSE model, the real-space similarity transformation fails. It transforms as $a_j \rightarrow (\sqrt{\frac{t+\gamma}{t-\gamma}})^i a_{Lj}, a_j^\dagger \rightarrow (\sqrt{\frac{t-\gamma}{t+\gamma}})^j a_{Rj}^\dagger$ (the same for b_j), which attaches the factor $(\frac{t+\gamma}{t-\gamma})^j$ to the pairing term $a_j b_j$ [see Eq. (3)] and breaks translational symmetry of the interacting Lindbladian.

In Fig. 2(a) we show the matrix elements of the real-space self-energy, given by each power of β in Eq. (6). In this plot, we rescale the matrix elements by $(\sqrt{\frac{t+\gamma}{t-\gamma}})^r$ to signify their competition between the original NHSE, where r is the hopping range. As shown by the plot, the scaled right hopping

strength (orange bars) dominates the left one (blue bars) as $|r|$ increases. Notice that for $\gamma > 0$, the right hopping strength of the unperturbed damping matrix already exceeds the left one. Therefore, interactions, whether repulsive or attractive, enhance NHSE of quasi-particles via the self-energy. We emphasize that the enhancement of single-particle NHSE seemingly contrasts with previous findings [34, 36, 39, 40, 71], as they focused on the non-Hermitian Hamiltonian but not the full-fledged open quantum dynamics governed by the Liouvillian. We also apply Eq. (8) to compute the self-energy corrections to eigenstates and compare it with ED in Fig. 2(b). Here, the x -axis only covers half of the Brillouin zone from 0 to π , because an eigenstate of this model is the equal-weight superposition of two non-Bloch waves with a pair of conjugate complex momentum $\sqrt{\frac{t+\gamma}{t-\gamma}} \exp(\pm i\theta)$ and thus opposite θ . Notably, our analytical formula agrees well with the numerical ED results. Furthermore, in Fig. 2(c), we perform finite-size scaling at $\theta = \pi/2$, where the self-energy real part is the largest (thus determining the Liouvillian gap), so as the deviation from ED. Remarkably, the theoretical value lies at the end of the linearly fitting curve of ED. Moreover, the $1/N$ scaling of finite-size corrections agrees with our semi-quantitative demonstration on Eq. (9). In the supplementary material [67], we consider a model with non-circular GBZ, and the results support our method.

Our self-energy formula can be applied with equal effectiveness to systems with PBC, where momentum k becomes a good quantum number. In this case, we should take $\beta = \exp(ik)$ in Eq. (8). In Fig. 3, we compare the self-energy for the same model with different boundary conditions, explicitly showing the boundary sensitivity. Notably for PBC, the spectrum of quasi-particles before perturbations is gapless at $k = -\pi/2$, and interactions open a gap which scales as U^2 . This is in sharp contrast to the common wisdom for closed 1D systems, where weak interactions are usually non-perturbative and drive the system to the Luttinger liquid phase, characterized by collective low-lying excitations. We elucidate the differences through a detailed analysis of the integral formula at the gapless point: to consider the “low-energy” regime near the singularity $(k_1, k_2) = (-\pi/2, -\pi/2)$, we introduce the infrared variables $p_{1(2)} = k_{1(2)} + \pi/2$, then the integral is approximated as $\sim \frac{u^2}{\gamma} \int dp_1 dp_2 \frac{(p_1^2 - p_2^2) - \frac{1}{2} p_1^2 (p_1^2 - p_2^2)}{p_1^2 + p_2^2 + p_1 p_2}$. The denominator is of the second order and is symmetric with respect to p_1 and p_2 . In the numerator, the leading asymmetric term vanishes, while the next term is of the fourth order which leads to no divergence. The differences between dissipative and closed systems are mainly rooted in the presence of complex spectrum in the former case.

Conclusions—In summary, we have presented a closed-form integral formula for the self-energy of fermionic non-Bloch modes in open quantum systems. Our analysis explicitly shows that the non-Hermitian skin effect leads to complex momentum propagators in the Feynman diagrams when evaluating the self-energy. By imposing complex momentum conservation, we further obtain a computable integral formula,

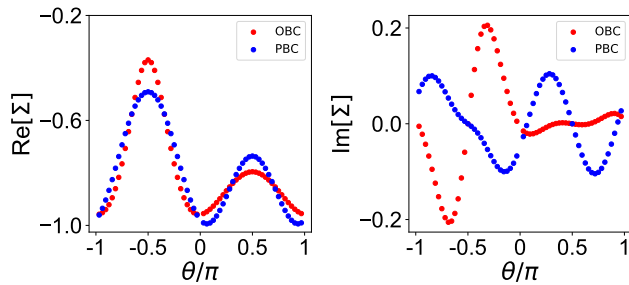


FIG. 3. Analytical results of the self-energy for different boundary conditions, as a function of angle of β on GBZ (OBC, red dots) and of the momentum (PBC, blue dots). $t = 1, \gamma = 0.5$.

which is consistent with numerical results. Our study establishes a general framework to analyze the interactions in open quantum systems using non-Bloch band theory, which leads to fermionic dissipative quasi-particles. Future research could aim at developing the non-Bloch self-energy for multi-band and higher-dimension systems [72–75]. It would also be interesting to investigate the localization transition of quasi-particles in the strongly interacting regime.

Acknowledgments—We thank Fei Song, Xu-Dong Dai, Dong Yuan, Yu-Min Hu, and Spenser Talkington for helpful discussions. This work was supported by the National Natural Science Foundation of China (Grant No. 12125405), and National Key R&D Program of China (No. 2023YFA1406702).

* These authors contributed equally to this work.

† wangzhongemail@tsinghua.edu.cn

- [1] S. Yao and Z. Wang, “Edge states and topological invariants of non-hermitian systems,” *Phys. Rev. Lett.* **121**, 086803 (2018).
- [2] F. K. Kunst, E. Edvardsson, J. C. Budich, and E. J. Bergholtz, “Biorthogonal bulk-boundary correspondence in non-hermitian systems,” *Phys. Rev. Lett.* **121**, 026808 (2018).
- [3] V. M. Martinez Alvarez, J. E. Barrios Vargas, and L. E. F. Foa Torres, “Non-hermitian robust edge states in one dimension: Anomalous localization and eigenspace condensation at exceptional points,” *Phys. Rev. B* **97**, 121401 (2018).
- [4] C. H. Lee and R. Thomale, “Anatomy of skin modes and topology in non-hermitian systems,” *Phys. Rev. B* **99**, 201103 (2019).
- [5] L. Xiao, T. Deng, K. Wang, G. Zhu, Z. Wang, W. Yi, and P. Xue, “Non-hermitian bulk–boundary correspondence in quantum dynamics,” *Nat. Phys.* **16**, 761 (2020).
- [6] T. Helbig, T. Hofmann, S. Imhof, M. Abdelghany, T. Kiessling, L. Molenkamp, C. Lee, A. Szameit, M. Greiter, and R. Thomale, “Generalized bulk–boundary correspondence in non-hermitian topoelectrical circuits,” *Nat. Phys.* **16**, 747 (2020).
- [7] A. Ghatak, M. Brandenbourger, J. van Wezel, and C. Coulais, “Observation of non-hermitian topology and its bulk–edge correspondence in an active mechanical metamaterial,” *Natl. Acad. Sci. U.S.A* **117**, 29561 (2020).
- [8] W. Wang, X. Wang, and G. Ma, “Non-Hermitian morphing of topological modes,” *Nature* **608**, 50 (2022), [arXiv:2203.02147](https://arxiv.org/abs/2203.02147) [[physics.app-ph](https://arxiv.org/abs/2203.02147)].
- [9] Y. Ashida, Z. Gong, and M. Ueda, “Non-hermitian physics,” *Adv. Phys.* **69**, 249 (2020).
- [10] H. Wang, J. Zhong, and S. Fan, “Non-hermitian photonic band winding and skin effects: a tutorial,” *Adv. Opt. Photon.* **16**, 659 (2024).
- [11] J. T. Gohsrich, A. Banerjee, and F. K. Kunst, “The non-hermitian skin effect: A perspective,” [arXiv:2410.23845](https://arxiv.org/abs/2410.23845).
- [12] K. Yokomizo and S. Murakami, “Non-bloch band theory of non-hermitian systems,” *Phys. Rev. Lett.* **123**, 066404 (2019).
- [13] S. Longhi, “Probing non-hermitian skin effect and non-bloch phase transitions,” *Phys. Rev. Res.* **1**, 023013 (2019).
- [14] F. Song, S. Yao, and Z. Wang, “Non-hermitian topological invariants in real space,” *Phys. Rev. Lett.* **123**, 246801 (2019).
- [15] K. Kawabata, N. Okuma, and M. Sato, “Non-bloch band theory of non-hermitian hamiltonians in the symplectic class,” *Phys. Rev. B* **101**, 195147 (2020).
- [16] S. Longhi, “Non-bloch-band collapse and chiral zener tunneling,” *Phys. Rev. Lett.* **124**, 066602 (2020).
- [17] Z. Yang, K. Zhang, C. Fang, and J. Hu, “Non-hermitian bulk-boundary correspondence and auxiliary generalized brillouin zone theory,” *Phys. Rev. Lett.* **125**, 226402 (2020).
- [18] C. H. Lee, L. Li, R. Thomale, and J. Gong, “Unraveling non-hermitian pumping: Emergent spectral singularities and anomalous responses,” *Phys. Rev. B* **102**, 085151 (2020).
- [19] Y. Yi and Z. Yang, “Non-hermitian skin modes induced by on-site dissipations and chiral tunneling effect,” *Phys. Rev. Lett.* **125**, 186802 (2020).
- [20] W.-T. Xue, M.-R. Li, Y.-M. Hu, F. Song, and Z. Wang, “Simple formulas of directional amplification from non-bloch band theory,” *Phys. Rev. B* **103**, L241408 (2021).
- [21] Y.-M. Hu, H.-Y. Wang, Z. Wang, and F. Song, “Geometric origin of non-bloch \mathcal{PT} symmetry breaking,” *Phys. Rev. Lett.* **132**, 050402 (2024).
- [22] B. Li, H.-R. Wang, F. Song, and Z. Wang, “Non-bloch dynamics and topology in a classical nonequilibrium process,” *Phys. Rev. B* **109**, L201121 (2024).
- [23] K. Zhang, Z. Yang, and C. Fang, “Correspondence between winding numbers and skin modes in non-hermitian systems,” *Phys. Rev. Lett.* **125**, 126402 (2020).
- [24] S. Mu, C. H. Lee, L. Li, and J. Gong, “Emergent fermi surface in a many-body non-hermitian fermionic chain,” *Phys. Rev. B* **102**, 081115 (2020).
- [25] K. Yang, S. C. Morampudi, and E. J. Bergholtz, “Exceptional spin liquids from couplings to the environment,” *Phys. Rev. Lett.* **126**, 077201 (2021).
- [26] K. Suthar, Y.-C. Wang, Y.-P. Huang, H. H. Jen, and J.-S. You, “Non-hermitian many-body localization with open boundaries,” *Phys. Rev. B* **106**, 064208 (2022).
- [27] Y.-M. Hu, W.-T. Xue, F. Song, and Z. Wang, “Steady-state edge burst: From free-particle systems to interaction-induced phenomena,” *Phys. Rev. B* **108**, 235422 (2023).
- [28] S. Longhi, “Spectral structure and doublon dissociation in the two-particle non-hermitian hubbard model,” *Annalen der Physik* **535**, 2300291 (2023).
- [29] T. Yoshida, S.-B. Zhang, T. Neupert, and N. Kawakami, “Non-hermitian mott skin effect,” *Phys. Rev. Lett.* **133**, 076502 (2024).
- [30] S. Hamanaka, K. Yamamoto, and T. Yoshida, “Interaction-induced liouvillian skin effect in a fermionic chain with a two-body loss,” *Phys. Rev. B* **108**, 155114 (2023).
- [31] J. Gliozzi, G. De Tomasi, and T. L. Hughes, “Many-body non-hermitian skin effect for multipoles,” *Phys. Rev. Lett.* **133**, 136503 (2024).
- [32] Y. Qin and L. Li, “Occupation-dependent particle separation in

- one-dimensional non-hermitian lattices,” *Phys. Rev. Lett.* **132**, 096501 (2024).
- [33] J. Gliozzi, G. De Tomasi, and T. L. Hughes, “Many-body non-hermitian skin effect for multipoles,” *Phys. Rev. Lett.* **133**, 136503 (2024).
- [34] P. Brighi and A. Nunnenkamp, “Nonreciprocal dynamics and the non-hermitian skin effect of repulsively bound pairs,” *Phys. Rev. A* **110**, L020201 (2024).
- [35] E. Lee, H. Lee, and B.-J. Yang, “Many-body approach to non-hermitian physics in fermionic systems,” *Phys. Rev. B* **101**, 121109 (2020).
- [36] T. Liu, J. J. He, T. Yoshida, Z.-L. Xiang, and F. Nori, “Non-hermitian topological mott insulators in one-dimensional fermionic superlattices,” *Phys. Rev. B* **102**, 235151 (2020).
- [37] K. Kawabata, K. Shiozaki, and S. Ryu, “Many-body topology of non-hermitian systems,” *Phys. Rev. B* **105**, 165137 (2022).
- [38] W. Chen, L. Peng, H. Lu, and X. Lu, “Characterizing bulk-boundary correspondence of one-dimensional non-hermitian interacting systems by edge entanglement entropy,” *Phys. Rev. B* **105**, 075126 (2022).
- [39] T. Yoshida and Y. Hatsugai, “Reduction of one-dimensional non-hermitian point-gap topology by interactions,” *Phys. Rev. B* **106**, 205147 (2022).
- [40] F. Alsallom, L. Herviou, O. V. Yazyev, and M. Brzezińska, “Fate of the non-hermitian skin effect in many-body fermionic systems,” *Phys. Rev. Res.* **4**, 033122 (2022).
- [41] S.-B. Zhang, M. M. Denner, T. c. v. Bzdušek, M. A. Sentef, and T. Neupert, “Symmetry breaking and spectral structure of the interacting hatano-nelson model,” *Phys. Rev. B* **106**, L121102 (2022).
- [42] B. H. Kim, J.-H. Han, and M. J. Park, “Collective non-hermitian skin effect: point-gap topology and the doublon-holon excitations in non-reciprocal many-body systems,” *Communications Physics* **7**, 73 (2024).
- [43] Y. Yi and Z. Yang, “Non-hermitian skin modes induced by on-site dissipations and chiral tunneling effect,” *Phys. Rev. Lett.* **125**, 186802 (2020).
- [44] N. Okuma and M. Sato, “Non-hermitian skin effects in hermitian correlated or disordered systems: Quantities sensitive or insensitive to boundary effects and pseudo-quantum-number,” *Phys. Rev. Lett.* **126**, 176601 (2021).
- [45] T. Yoshida, “Real-space dynamical mean field theory study of non-hermitian skin effect for correlated systems: Analysis based on pseudospectrum,” *Phys. Rev. B* **103**, 125145 (2021).
- [46] H. Geng, J. Y. Wei, M. H. Zou, L. Sheng, W. Chen, and D. Y. Xing, “Nonreciprocal charge and spin transport induced by non-hermitian skin effect in mesoscopic heterojunctions,” *Phys. Rev. B* **107**, 035306 (2023).
- [47] S. Kaneshiro, T. Yoshida, and R. Peters, “ Z_2 non-hermitian skin effect in equilibrium heavy-fermion systems,” *Phys. Rev. B* **107**, 195149 (2023).
- [48] T. Micallo, C. Lehmann, and J. C. Budich, “Correlation-induced sensitivity and non-hermitian skin effect of quasiparticles,” *Phys. Rev. Res.* **5**, 043105 (2023).
- [49] H.-R. Wang, B. Li, F. Song, and Z. Wang, “Scale-free non-hermitian skin effect in a boundary-dissipated spin chain,” *SciPost Phys.* **15**, 191 (2023).
- [50] T. Guo, K. Kawabata, R. Nakai, and S. Ryu, “Non-hermitian boost deformation,” *Phys. Rev. B* **108**, 075108 (2023).
- [51] M. Zheng, Y. Qiao, Y. Wang, J. Cao, and S. Chen, “Exact solution of the bose-hubbard model with unidirectional hopping,” *Phys. Rev. Lett.* **132**, 086502 (2024).
- [52] C. H. Lee, “Many-body topological and skin states without open boundaries,” *Phys. Rev. B* **104**, 195102 (2021).
- [53] R. Shen and C. H. Lee, “Non-hermitian skin clusters from strong interactions,” *Commun Phys* **5**, 238 (2022).
- [54] W. N. Faugno and T. Ozawa, “Interaction-induced non-hermitian topological phases from a dynamical gauge field,” *Phys. Rev. Lett.* **129**, 180401 (2022).
- [55] H. Li, H. Wu, W. Zheng, and W. Yi, “Many-body non-hermitian skin effect under dynamic gauge coupling,” *Phys. Rev. Res.* **5**, 033173 (2023).
- [56] L. Mao, Y. Hao, and L. Pan, “Non-hermitian skin effect in a one-dimensional interacting bose gas,” *Phys. Rev. A* **107**, 043315 (2023).
- [57] Y. Wang, X. Zhang, Z. Yang, and C. Wu, “An explicit wavefunction of the interacting non-hermitian spin-1/2 1d system,” arXiv:2409.04112 .
- [58] G. Chen, F. Song, and J. L. Lado, “Topological spin excitations in non-hermitian spin chains with a generalized kernel polynomial algorithm,” *Phys. Rev. Lett.* **130**, 100401 (2023).
- [59] S. E. Begg and R. Hanai, “Quantum criticality in open quantum spin chains with nonreciprocity,” *Phys. Rev. Lett.* **132**, 120401 (2024).
- [60] H.-P. Breuer, F. Petruccione, *et al.*, *The theory of open quantum systems* (Oxford University Press on Demand, 2002).
- [61] F. Song, S. Yao, and Z. Wang, “Non-hermitian skin effect and chiral damping in open quantum systems,” *Phys. Rev. Lett.* **123**, 170401 (2019).
- [62] T. Haga, M. Nakagawa, R. Hamazaki, and M. Ueda, “Liouvillian skin effect: Slowing down of relaxation processes without gap closing,” *Phys. Rev. Lett.* **127**, 070402 (2021).
- [63] F. Yang, Q.-D. Jiang, and E. J. Bergholtz, “Liouvillian skin effect in an exactly solvable model,” *Phys. Rev. Res.* **4**, 023160 (2022).
- [64] G. Lee, A. McDonald, and A. Clerk, “Anomalously large relaxation times in dissipative lattice models beyond the non-hermitian skin effect,” *Phys. Rev. B* **108**, 064311 (2023).
- [65] M. Schmutz, “Real-time green’s functions in many body problems,” *Z Physik B* **30**, 97 (1978).
- [66] A similar formalism, including the parity operator η , has been adopted in Refs. [76–79].
- [67] See the Supplementary Materials at [URL will be inserted by publisher] for the fermionic bi-base mapping, the exact form of the steady state, the self-energy formula for generic Z -matrices, calculations of the coefficients in the eigenstate wavefunctions based on the boundary equations, scaling analysis of the non-Bloch self-energy, and more analytical and numerical results of different models.
- [68] N. Hatano and D. R. Nelson, “Localization transitions in non-hermitian quantum mechanics,” *Phys. Rev. Lett.* **77**, 570 (1996).
- [69] N. Hatano and D. R. Nelson, “Vortex pinning and non-hermitian quantum mechanics,” *Phys. Rev. B* **56**, 8651 (1997).
- [70] N. Hatano and D. R. Nelson, “Non-hermitian delocalization and eigenfunctions,” *Phys. Rev. B* **58**, 8384 (1998).
- [71] B. Dóra and C. u. u. u. P. m. c. Moca, “Full counting statistics in the many-body hatano-nelson model,” *Phys. Rev. B* **106**, 235125 (2022).
- [72] K. Zhang, Z. Yang, and C. Fang, “Universal non-hermitian skin effect in two and higher dimensions,” *Nat. Commun.* **13**, 2496 (2022).
- [73] Y.-M. Hu and Z. Wang, “Green’s functions of multiband non-hermitian systems,” *Phys. Rev. Res.* **5**, 043073 (2023).
- [74] H.-Y. Wang, F. Song, and Z. Wang, “Amoeba formulation of non-bloch band theory in arbitrary dimensions,” *Phys. Rev. X* **14**, 021011 (2024).
- [75] K. Zhang, C. Shu, and K. Sun, “Algebraic non-hermitian skin effect and unified non-bloch band theory in arbitrary dimen-

- sions,” [arXiv:2406.06682](#) .
- [76] T. Prosen, “Third quantization: a general method to solve master equations for quadratic open fermi systems,” *New J. Phys.* **10**, 043026 (2008).
- [77] T. Prosen, “Spectral theorem for the lindblad equation for quadratic open fermionic systems,” *J. Stat. Mech.* **2010**, P07020 (2010).
- [78] T. Barthel and Y. Zhang, “Solving quasi-free and quadratic lindblad master equations for open fermionic and bosonic systems,” *J. Stat. Mech.* **2022**, 113101 (2022).
- [79] A. McDonald and A. A. Clerk, “Third quantization of open quantum systems: Dissipative symmetries and connections to phase-space and keldysh field-theory formulations,” *Phys. Rev. Res.* **5**, 033107 (2023).

Supplementary Material for: Non-Bloch self-energy of dissipative interacting fermions

He-Ran Wang,^{1,*} Zijian Wang,^{1,*} and Zhong Wang^{1,†}

¹*Institute for Advanced Study, Tsinghua University, Beijing 100084, People's Republic of China*

I. THE FRAMEWORK OF FREE-FERMION LIOUVILLIAN

A. Fermionic bi-base mapping

In this subsection, we will work out the formulation of the free-fermionic Liouvillian in detail. To map the fermionic Liouvillian to a rank-2 non-Hermitian Hamiltonian, we apply the bi-base mapping. The mapping of operators on the Fock basis is given by:

$$\begin{aligned} |m\rangle\langle n| &\rightarrow |m\rangle \otimes |n\rangle, \quad c_i^\dagger |m\rangle\langle n| \rightarrow c_i^\dagger |m\rangle \otimes |n\rangle, \quad c_i |m\rangle\langle n| \rightarrow c_i |m\rangle \otimes |n\rangle, \\ |m\rangle\langle n| c_i &\rightarrow \bar{c}_i^\dagger |m\rangle \otimes |n\rangle, \quad |m\rangle\langle n| c_i^\dagger \rightarrow \bar{c}_i |m\rangle \otimes |n\rangle. \end{aligned} \quad (S1)$$

However, under such mapping, fermionic operators on different sides of density matrix c_i and \bar{c}_j commutes with each other, $[c_i, \bar{c}_j] = 0$. To impose mutual fermionic statistics, we introduce the Klein factor before \bar{c} and \bar{c}^\dagger operators as in the literature of bosonization [1]: $\bar{c}_i \rightarrow K \bar{c}_i$, $K = \prod_i (-1)^{n_i + \bar{n}_i}$. Then, we have the desired mutual statistics

$$\{c_i, \bar{c}_j\} = c_i \bar{c}_j + \bar{c}_j c_i = -K c_i K \bar{c}_j + K K \bar{c}_j c_i = -K [c_i, K \bar{c}_j] = 0. \quad (S2)$$

Next, we decompose K to $\eta \bar{\eta}$, where $\eta = \prod_i (-1)^{n_i}$ [$\bar{\eta} = \prod_i (-1)^{\bar{n}_i}$] is the fermionic parity operator for left (right) fermions. Following the mapping rule, we obtain the double-space representation of the quadratic Liouvillian as the main text:

$$\mathcal{L}_0 = \mathbf{c}^\dagger \mathbb{L}_0 \mathbf{c} - \text{Tr}(M^l + (M^g)^T - ih), \quad \mathbb{L}_0 = \begin{pmatrix} -ih + (M^g)^T - M^l & 2(M^g)^T \\ 2M^l & -ih - (M^g)^T + M^l \end{pmatrix}. \quad (S3)$$

The $2N \times 2N$ matrix \mathbb{L}_0 , as the first quantized Liouvillian, can be block diagonalized by a similarity transformation. In the following, we will demonstrate how to construct the transformation matrix stepwisely.

First, we apply the unitary transformation $H = \frac{1}{\sqrt{2}} \begin{pmatrix} I & I \\ I & -I \end{pmatrix}$ (notation ‘‘H’’ comes from the Hadamard gate) to block-lower-diagonalize the \mathbb{L}_0 :

$$H \mathbb{L}_0 H^{-1} = \begin{pmatrix} -X^\dagger & 0 \\ 2[(M^g)^T - M^l] & X \end{pmatrix}. \quad (S4)$$

We have a few remarks on the similarities between the unitary transformation H and the Keldysh rotation in the context of non-equilibrium field theory:

- Both have two copies of the original system: for the Liouvillian they are left and right fermions, while for Keldysh field theory they are forward and backward fields in the time direction;
- The Hadamard matrix and the Keldysh rotation share the same form;
- After the transformation, one of the blocks (the τ^+ block) becomes zero, and two of the blocks are anti-Hermitian conjugate pair.

Next, as the standard approach to diagonalizing lower-triangle matrices, we introduce the transformation $T = \begin{pmatrix} I & 0 \\ Z & I \end{pmatrix}$ which acts as

$$\begin{pmatrix} I & 0 \\ Z & I \end{pmatrix} \begin{pmatrix} -X^\dagger & 0 \\ 2[(M^g)^T - M^l] & X \end{pmatrix} \begin{pmatrix} I & 0 \\ -Z & I \end{pmatrix} = \begin{pmatrix} -X^\dagger & 0 \\ 2[(M^g)^T - M^l] - XZ - ZX^\dagger & X \end{pmatrix}. \quad (S5)$$

The matrix Z is determined by the condition that the off-diagonal block vanishes:

$$2[(M^g)^T - M^l] - XZ - ZX^\dagger = 0, \quad (S6)$$

which admits the form of the Lyapunov equation. Consequently, we obtain the desired similarity transformation S which block diagonalizes \mathbb{L}_0 :

$$S = TH = \frac{1}{\sqrt{2}} \begin{pmatrix} I & I \\ I + Z & -I + Z \end{pmatrix}, \quad S \mathbb{L}_0 S^{-1} = \begin{pmatrix} -X^\dagger & \\ & X \end{pmatrix}. \quad (S7)$$

B. The non-equilibrium steady state

Real part of the spectrum of the damping matrix X must be semi-definite negativity, characterizing the dissipative nature of the Liouvillian dynamics. The non-equilibrium steady state $|\rho_{ss}\rangle$, being the zero-eigenvalue eigenstate of the Liouvillian, is the vacuum of a and b quasi-particles:

$$a_{Lm}|\rho_{ss}\rangle = b_{Lm}|\rho_{ss}\rangle = 0, \quad \forall m. \quad (\text{S8})$$

For the quadratic Liouvillian, we propose the fermionic Gaussian state ansatz for the steady state (without normalization):

$$\rho_{ss} = \exp\left[\sum_{mn} (G)_{mn} c_m^\dagger c_n\right], \quad |\rho_{ss}\rangle = \exp\left[\sum_{mn} (e^G)_{mn} c_m^\dagger \bar{c}_n^\dagger\right]|0, 0\rangle, \quad (\text{S9})$$

where G is a Hermitian matrix to be decided, dubbed as the first quantized modular Hamiltonian. We diagonalize G as $G_{ij} = \sum_k V_{ki}^* V_{kj} g_k$ and define fermion operators $d_k = \sum_l V_{kl} c_l$, $\bar{d}_k = \sum_l V_{kl}^* \bar{c}_l$, then the steady state admits the canonical form:

$$|\rho_{ss}\rangle = \exp\left(\sum_k e^{g_k} d_k^\dagger \bar{d}_k^\dagger\right)|0, 0\rangle = \prod_k [(1 + e^{g_k}) d_k^\dagger \bar{d}_k^\dagger]|0, 0\rangle. \quad (\text{S10})$$

The state fulfills relations

$$(1 + e^{g_k}) \eta d_k |\rho_{ss}\rangle = (1 - e^{g_k}) \bar{d}_k^\dagger \bar{\eta} |\rho_{ss}\rangle, \quad (1 - e^{g_k}) d_k^\dagger \eta |\rho_{ss}\rangle = -(1 + e^{g_k}) \bar{\eta} \bar{d}_k |\rho_{ss}\rangle, \quad (\text{S11})$$

On the other hand, we can rewrite the annihilation condition (S8) by diagonalizing the matrix Z as $Z_{ij} = \sum_k W_{ki}^* W_{kj} z_k$, and define fermions: $f_k = \sum_l W_{kl} c_l$, $\bar{f}_k = \sum_l W_{kl}^* \bar{c}_l$, then we have

$$(1 + z_k) \eta f_k |\rho_{ss}\rangle = (1 - z_k) \bar{f}_k^\dagger \bar{\eta} |\rho_{ss}\rangle, \quad (1 - z_k) f_k^\dagger \eta |\rho_{ss}\rangle = -(1 + z_k) \bar{\eta} \bar{f}_k |\rho_{ss}\rangle. \quad (\text{S12})$$

Compare it with Eq. (S11), we can explicitly establish the relation between G and Z :

$$G = \ln\left[\frac{I - Z}{I + Z}\right]. \quad (\text{S13})$$

The normalization factor (partition function) of ρ_{ss} is given by

$$\mathcal{Z} = \text{Tr}(\rho_{ss}) = \prod_k \left(1 + \frac{1 - z_k}{1 + z_k}\right) = 2^N / \text{Det}(1 + Z). \quad (\text{S14})$$

In the main text we examine $Z = 0$ case, so the associate steady state is the identity, in accordance with the common knowledge that the Liouvillian dynamics with Hermitian dissipators (notice that dissipators are defined up to a unitary transformation over different channels) can induce decoherence and lead to the maximally mixed state.

C. Z -matrix for lattice models

From the above analysis, we find that the spectrum of free fermion Liouvillian fully depends on the damping matrix X , while Z -matrix decides the Gaussian steady state. In this subsection we will discuss the explicit form of the Z -matrix for lattice models under the open boundary condition, through solving the Lyapunov equation. Then we will develop the self-energy formula for a generic Z -matrix, as a complement to the results in main text.

Adopting bi-base mapping on the matrix Z to unfold it to a vector $|Z\rangle = \sum_{ij} Z_{ij} |i\rangle \otimes |j\rangle$, the Lyapunov equation is subsequently transformed to $(X \otimes I + I \otimes X^*)|Z\rangle = |M\rangle$, $M = 2((M^g)^T - M^l)$. Then we tend to take the inverse of $X \otimes I + I \otimes X^\dagger$ to evaluate Z . To this end, we decompose the factor on its eigenbasis as:

$$\begin{aligned} \left[\frac{1}{X \otimes I + I \otimes X^*}\right]_{ij, lk} &= \sum_{mn} \frac{1}{\lambda_m + \lambda_n^*} \langle i|u_{Rm}\rangle \langle u_{Lm}|j\rangle \langle k|u_{Ln}\rangle \langle u_{Rn}|l\rangle \\ &= \sum_m \langle i|u_{Rm}\rangle \langle u_{Lm}|j\rangle \sum_n \frac{\langle k|u_{Ln}\rangle \langle u_{Rn}|l\rangle}{\lambda_m + \lambda_n^*} \\ &= -\sum_m \langle i|u_{Rm}\rangle \langle u_{Lm}|j\rangle G_{lk}(-\lambda_m, X^*), \end{aligned} \quad (\text{S15})$$

here $X|u_{Rm}\rangle = \lambda_m|u_{Rm}\rangle$, $X^\dagger|u_{Lm}\rangle = \lambda_m^*|u_{Lm}\rangle$, and we have defined the single-particle Green's function $G_{ij}(z, X) = [\frac{1}{z-X}]_{ij}$. Before proceeding on, we introduce two formulas. The first one comes from the complex analysis:

$$\frac{\partial}{\partial z^*} \frac{1}{z} = \pi \delta(x) \delta(y) = \pi \delta(z), \quad (\text{S16})$$

here $z = x + iy$ is defined on the complex plane, and $\frac{\partial}{\partial z^*} = \frac{1}{2}(\frac{\partial}{\partial x} + i\frac{\partial}{\partial y})$. The other one is the formula of open boundary Green's function [2]:

$$G_{ij}(z, X) = \oint_{\text{GBZ}} \frac{d\beta}{2\pi i \beta} \frac{\beta^{i-j}}{z - X(\beta)}. \quad (\text{S17})$$

In general one should conduct the integral on a convergence circle, on which the complex function $z - X(\beta)$ has a vanishing winding number with respect to the zero point. Such a integral contour can always be replaced by the GBZ, since the image of $X(\beta)$ from the GBZ is indeed the spectrum of X under open boundary condition, which winds zero with respect to any point.

Then we calculate the matrix inverse utilizing the two formulas:

$$\begin{aligned} [\frac{1}{X \otimes I + I \otimes X^*}]_{ij, lk} &= - \int d^2 z [\delta(z - X)]_{ij} G_{lk}(-z, X^*) = - \int d^2 z [\frac{\partial}{\pi \partial z^*} G_{ij}(z, X)] G_{lk}(-z, X^*) \\ &= - \int d^2 z [\frac{\partial}{\pi \partial z^*} \oint_{\text{GBZ}} \frac{d\beta}{2\pi i \beta} \frac{\beta^{i-j}}{z - X(\beta)}] G_{lk}(-z, X^*) \\ &= - \int d^2 z \oint_{\text{GBZ}} \frac{d\beta}{2\pi i \beta} \beta^{i-j} \delta(z - X(\beta)) G_{lk}(-z, X^*) \\ &= \oint_{\text{GBZ}} \frac{d\beta}{2\pi i \beta} \oint_{\text{GBZ}^*} \frac{d\beta'}{2\pi i \beta'} \frac{\beta^{i-j} \beta'^{l-k}}{X(\beta) + X^*(\beta')} \\ &= \int_{-\infty}^{+\infty} \frac{d\omega}{2\pi} \oint_{\text{GBZ}} \frac{d\beta}{2\pi i \beta} \frac{\beta^{i-j}}{i\omega + X(\beta)} \oint_{\text{GBZ}^*} \frac{d\beta'}{2\pi i \beta'} \frac{\beta'^{l-k}}{i\omega - X^*(\beta')} \end{aligned} \quad (\text{S18})$$

From the first sight, the matrix inverse depends on the boundary condition. However, for fermionic systems the real part of $X(\beta)$ on the GBZ or BZ can never be positive due to the contractive nature of the Liouvillian, so we can freely deform the integral contour between the two. It turns out that at least for i, j deep in the bulk, the corresponding matrix elements of Z should be the same for PBC and OBC: $Z_{ij} = \oint \frac{dk}{2\pi} Z(k) e^{ik(i-j)}$.

In the main text we assume $(M^g)^T = M^l$ for simplicity. For the generic case $(M^g)^T \neq M^l$, we can show that

$$n_i - \bar{n}_i = a_{Ri}^\dagger a_{Li} - b_{Ri}^\dagger b_{Li}, \quad (\text{S19})$$

and

$$n_i + \bar{n}_i = 1 - Z_{ii} + \sum_j (Z_{ij} b_{Rj}^\dagger b_{Li} + Z_{ji} a_{Rj}^\dagger a_{Li}) + b_{Li} a_{Li} + a_{Ri}^\dagger b_{Ri}^\dagger - \sum_{jk} Z_{ij} Z_{ik} a_{Rj}^\dagger b_{Rk}^\dagger, \quad (\text{S20})$$

so that the second-order perturbation term in the real space is given by

$$\langle i_a | \mathcal{L}_{\text{eff}}^{(2)} | j_a \rangle = -\frac{1}{4} (\sum_{kl} U_{ik} U_{jl} - \sum_{knlm} U_{ik} U_{jn} Z_{nl} Z_{nm}) \oint_{\text{GBZ}} \frac{d\beta_1}{2\pi i \beta_1} \oint_{\text{GBZ}} \frac{d\beta_2}{2\pi i \beta_2} \oint_{\text{GBZ}} \frac{d\beta_3}{2\pi i \beta_3} \frac{(\beta_1^{i-j} \beta_2^{k-l} - \beta_1^{i-l} \beta_2^{k-j}) \beta_3^{k-l}}{E - X(\beta_1) - X(\beta_2) - X^*(\beta_3)}. \quad (\text{S21})$$

We can write the matrix Z to the non-Bloch form by adopting the translational invariant. As a result, in the non-Bloch self-energy formula, an additional prefactor $1 - Z(\beta_2)Z(\beta_3)$ should be attached:

$$\Sigma^{(2)}(E, \beta) = -\frac{1}{4} \oint_{\text{GBZ}} \frac{d\beta_1}{2\pi i \beta_1} \oint_{\text{GBZ}} \frac{d\beta_2}{2\pi i \beta_2} \oint_{\text{GBZ}^*} \frac{d\beta_3}{2\pi i \beta_3} \sum_r (\frac{\beta_1 \beta_2 \beta_3}{\beta})^r \times [1 - Z(\beta_2)Z(\beta_3)] \frac{U(\beta_2 \beta_3)^2 - U(\beta_2 \beta_3)U(\beta_1 \beta_3)}{E - X(\beta_1) - X(\beta_2) - X^*(\beta_3)}. \quad (\text{S22})$$

II. WEIGHTED AVERAGE OF THE NON-BLOCH SELF-ENERGY

A. NHSE eigenstates and the boundary condition

For 1D open boundary lattice models without disorders, the generic single-band non-Hermitian Hamiltonian has the form $H = \sum_i \sum_{l=-M}^M t_l |i\rangle \langle i+l|$, where M is the hopping range. For brevity here we only discuss the symmetric hopping range. We take an ansatz for the (right) eigenstate of H with the eigen-energy E as $|R\rangle = \sum_{\mu=1}^{2M} \sum_{i=1}^N \phi_{\mu}^R \beta_{\mu}^i |i\rangle = \sum_{i=1}^N \psi_i |i\rangle$, where β_{μ} are $2M$ solutions of the characteristic equation $E = H(\beta) = \sum_{l=-M}^M t_l \beta^{-l}$, ordered by their modulus. The coefficients ϕ_{μ}^R are fixed by imposing the open boundary condition such that $\psi_{1-\mu} = \psi_{N+\mu} = 0, \mu = 1, \dots, M$. Thus We obtain $2M$ equations of ϕ_{μ}^R as

$$\sum_{\mu=1}^{2M} \beta_{\mu}^{1-\nu} \phi_{\mu}^R = 0, \quad \sum_{\mu=1}^{2M} \beta_{\mu}^{N+\nu} \phi_{\mu}^R = 0, \quad \nu = 1, \dots, M. \quad (\text{S23})$$

Linear equations of ϕ_{μ}^L can also be derived following the same method.

According to the non-Bloch band theory [3], for an eigen-energy E , among the roots of the equation $H(\beta) = E$, we have $|\beta_M| = |\beta_{M+1}|$. If we choose $\phi_{\mu}^R, \phi_{\mu}^L$ to be $\mathcal{O}(1)$ when $\mu = M, M+1$, fulfilling the boundary condition requires that $\phi_{\mu}^{R(L)} \sim \mathcal{O}(1)$ for $\mu < M (\mu > M+1)$ and $\phi_{\mu}^{R(L)} \sim \mathcal{O}(|\frac{\beta_M}{\beta_{\mu}}|^N) (\mathcal{O}(|\frac{\beta_{\mu}}{\beta_M}|^N))$ for $\mu > M+1 (\mu < M)$. Notice that with disordered terms on the boundary, the explicit form of the boundary equations will be changed, though the above conclusions about the scaling behavior of the coefficients are still preserved.

B. Scaling analysis for the self-energy

By definition, the second-order energy shift for an eigenstate $|R\rangle$ of the damping matrix is $\langle L | \hat{\Sigma}^{(2)}(E) | R \rangle / \langle L | R \rangle$. Utilizing the periodicity of the self-energy matrix elements $\Sigma_{ij}^{(2)}$, we can express the expectation value of self-energy as a summation of $\Sigma^{(2)}(\beta_{\mu})$ over $\mu = 1$ to $2M$, with different weights:

$$\langle L | \hat{\Sigma}^{(2)}(E) | R \rangle = \sum_{\mu\nu}^{2M} [\phi_{\mu}^R \phi_{\nu}^L \Sigma^{(2)}(\beta_{\mu}, E) \sum_{j=1}^N (\beta_{\mu}/\beta_{\nu})^j] \equiv \sum_{\mu\nu}^{2M} \sigma_{\mu,\nu}. \quad (\text{S24})$$

We will prove that in the thermodynamic limit, among all pairs of index μ, ν , two of them $\sigma_{M,M}, \sigma_{M+1,M+1}$ dominate the others.

Given the relative magnitude of different β_{μ} in the above subsection, the scaling behavior of those terms in (S24) categorized into five distinct scenarios:

- $\mu = \nu = M, \sigma_{M,M} = N \phi_M^R \phi_M^L \Sigma^{(2)}(\beta_M, E)$. Similarly, $\sigma_{M+1,M+1} = N \phi_{M+1}^R \phi_{M+1}^L \Sigma^{(2)}(\beta_{M+1}, E)$, and the two terms are of the same order $\sim \mathcal{O}(N)$.
- $\mu = M, \nu = M+1$ or $\mu = M+1, \nu = M$. Define $e^{i\phi} = \beta_{M+1}/\beta_M$, in $\sigma_{\mu,\nu}$ the summation $\sum_{j=1}^N (e^{\pm i\phi})^j$ goes to zero in the thermodynamic limit, since $\beta_M \neq \beta_{M+1}$ in general.
- $\mu = \nu \neq M, M+1$. If $\mu > M+1$ then $\sigma_{\mu,\mu} \sim N |\frac{\beta_M}{\beta_{\mu}}|^N$, otherwise $\mu < M$ and $\sigma_{\mu,\mu} \sim N |\frac{\beta_{\mu}}{\beta_M}|^N$, both is much smaller than the first case.
- $\mu > \nu$ and $|\beta_{\mu}| \neq |\beta_{\nu}|$. If $\mu \leq M+1$, we have $\phi_{\mu}^R \sim \mathcal{O}(1), \phi_{\nu}^L \sim |\beta_{\nu}/\beta_M|^N$, so $\sigma_{\mu,\nu} \sim |\beta_{\mu}/\beta_M|^N$. If $\mu > M+1$ and $\nu < M, \sigma_{\mu,\nu} \sim \mathcal{O}(1)$. Otherwise, $\nu \geq M$ and $\sigma_{\mu,\nu} \sim |\beta_M/\beta_{\nu}|^N$. All of them are much smaller than $\mathcal{O}(N)$.
- $\mu < \nu$ and $|\beta_{\mu}| \neq |\beta_{\nu}|$. The analysis is very similar with the previous one, so as the conclusion.

The above qualitative analysis shows that the largest terms in the self-energy scales as $\mathcal{O}(N)$ (without normalization), contributed by $\sigma_{M,M} + \sigma_{M+1,M+1}$, while other terms scale as $\mathcal{O}(1)$ at most. Therefore, the error of our formula scales as $\mathcal{O}(1/N)$. Adding the normalization factor, a closed form eigenstate self-energy is given by:

$$\langle L | \hat{\Sigma}^{(2)}(E) | R \rangle \simeq (\phi_M^R \phi_M^L \Sigma^{(2)}(\beta_M, E) + \phi_{M+1}^R \phi_{M+1}^L \Sigma^{(2)}(\beta_{M+1}, E)) / (\phi_M^R \phi_M^L + \phi_{M+1}^R \phi_{M+1}^L). \quad (\text{S25})$$

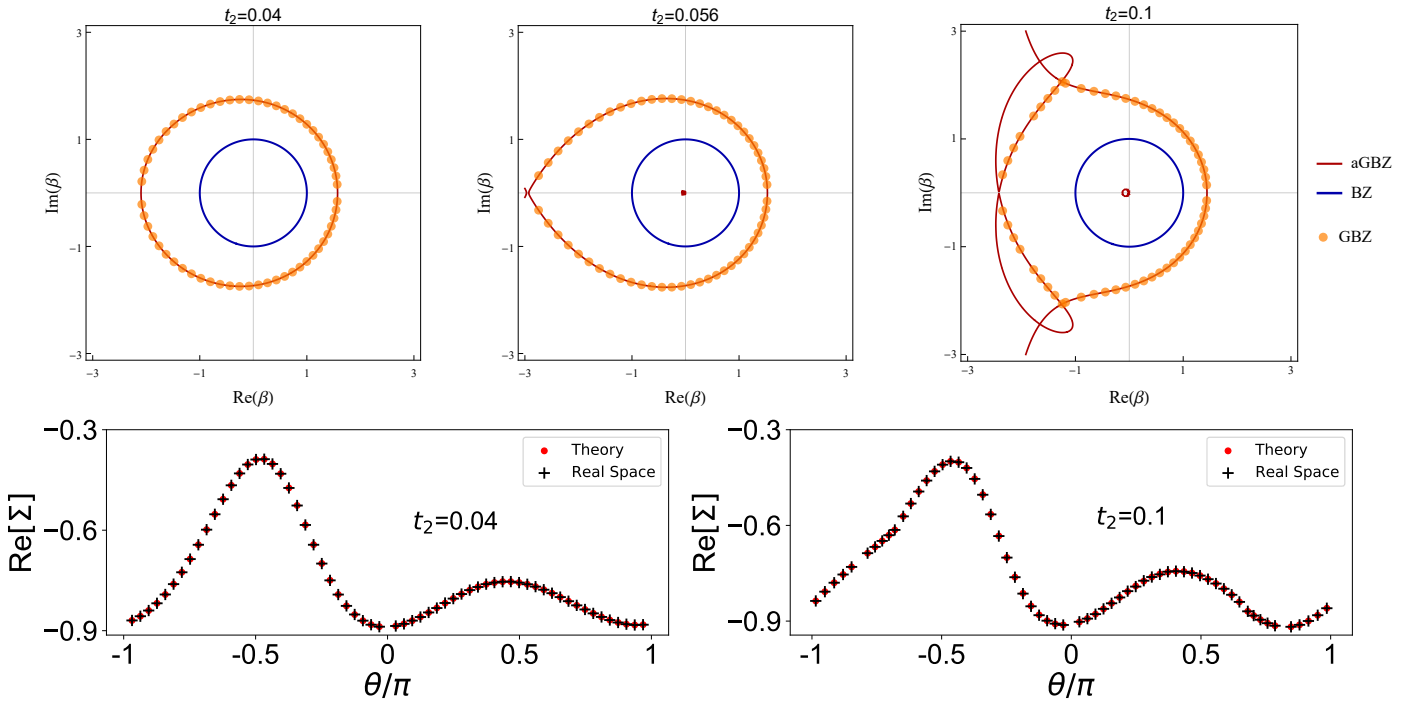


FIG. S1. GBZ is presented in the three figures from the first row. Three values of next-nearest-neighbor hopping t_2 are taken. They are before, at and after the PT symmetry transition of the energy spectrum, respectively. Red curves denote auxiliary GBZ (aGBZ) while orange points (GBZ) stick on them, obtained from exact diagonalization of a finite system. As a comparison, BZ is plotted in blue. Two figures in the second row show numerical results of self-energy at $t_2 = 0.04$ and 0.1 .

III. NUMERICAL RESULTS FOR OTHER MODELS

We apply the non-Bloch self-energy formula to the model with next-nearest-neighbor hopping of strength t_2 , for which the analytical integral on the GBZ meets challenges. The damping matrix is $X(\beta) = -\gamma_0 - i(t-\gamma)\beta - i(t+\gamma)\beta^{-1} - it_2(\beta^2 + \beta^{-2})$. Turning on t_2 from 0, when it is smaller than a critical value, the spectrum of the damping matrix remains being a straight line accompanying with the GBZ deviating from the circle on the complex plane. After t_2 approaching t_{2c} , cusps appear on GBZ, and the spectrum undergoes PT-symmetry breaking and develops complex eigenvalues. We take $t = 1, \gamma = 0.5, \gamma_0 = 1.1$ so that $t_{2c} = 0.056$ [4]. The deformation of the GBZ as t_2 changes is shown in the first row of Fig.S1. In the second row, we compare the self-energy obtained from the real-space effective Hamiltonian and the integral formula on BZ, which match really well.

* These authors contributed equally to this work.

† wangzhongemail@tsinghua.edu.cn

- [1] J. Von Delft and H. Schoeller, “Bosonization for beginners refermionization for experts,” *Ann. Phys.* **510**, 225 (1998).
- [2] W.-T. Xue, M.-R. Li, Y.-M. Hu, F. Song, and Z. Wang, “Simple formulas of directional amplification from non-bloch band theory,” *Phys. Rev. B* **103**, L241408 (2021).
- [3] K. Yokomizo and S. Murakami, “Non-bloch band theory of non-hermitian systems,” *Phys. Rev. Lett.* **123**, 066404 (2019).
- [4] Y.-M. Hu, H.-Y. Wang, Z. Wang, and F. Song, “Geometric origin of non-bloch \mathcal{PT} symmetry breaking,” *Phys. Rev. Lett.* **132**, 050402 (2024).